

Parameterization of Electron Attachment Rate Constants for Impurities in LArTPC Detectors

Y. Li^a, *C. Bromberg^b, M. Diwan^a, S. Kettell^a, S. Martynenko^a, X. Qian^a, V. Paolone^c, J. Stewart^a, C. Thorn^a, and C. Zhang^a,

^aPhysics Department, Brookhaven National Laboratory, Upton, NY 11973, USA

^bDepartment of Physics and Astronomy, Michigan State University, East Lansing, MI 48824, USA

^cDepartment of Physics and Astronomy, University of Pittsburgh, Pittsburgh, PA 15260, USA

ABSTRACT: The ability of free electrons to drift long distances at high velocities in pure liquid argon under an applied electric field has been exploited for the past forty years to implement detectors with increasingly larger volumes for high energy physics research. In this paper, we summarize the electron attachment rate constants as a function of the external electric field for common impurities in LArTPC with data from the literature. We further provide analytical functions to parameterize the data, which are useful to compare with new measurements as well as to make extrapolations.

KEYWORDS: Liquid Argon; Electron Attachment; Purity; Impurities; Electron Lifetime.

*Corresponding author: yichen@bnl.gov

Contents

1. Introduction	1
2. Global Fit to existing Data	2
2.1 Data from the literature	2
2.2 Fitting Functions	5
3. Applications	6
4. Conclusions	10

1. Introduction

Liquid argon time projection chambers (LArTPC) and calorimetric detectors [1, 2, 3, 4] are widely used in neutrino [5, 6, 7, 8, 9, 10, 11] and dark matter experiments [12, 13, 14]. On the neutrino frontier, the short-baseline neutrino (SBN) [15] program and the Deep Underground Neutrino Experiment (DUNE) [16] will perform a precision search and measurement of neutrino oscillations with single-phase multiple LArTPCs, respectively. On the dark matter frontier, DarkSide-20k [17] will advance the search for direct dark matter detection with a dual-phase LArTPC.

For the detection of the ionization charge in LArTPCs, electron attachment to impurities in LAr (such as water or oxygen) is a source of signal attenuation, given that the drift velocity of ions is about five orders of magnitude lower than that of electrons [18]. This means that even transient or resonant attachment of an electron to form a negative ion with lifetimes longer than a fraction of the electron drift time will cause loss of signal.

Attachment to form a stable Ar^- ion has not been reported. Electron attachment to Ar, in the gas phase, has been observed to form excited states at 11.10 eV and 11.28 eV, both with lifetimes of about 10^{-16}s [19]. Since these energies are so far above the mean electron energy at the drift fields sustainable in LAr detectors and the lifetimes are so short compared to drift times, or even to electron collision times, direct attachment to argon effectively does not occur. It remains possible that in pure LAr other processes, such as attachment to clusters, might occur. However, for practical purposes, the lifetime of free electrons in pure LAr is so long that other factors, such as diffusion, would limit the ultimate useful drift time. Only attachment to impurities in the LAr needs to be considered.

Accurate knowledge and minimization of charge attenuation is critical for LArTPCs, since the collected charge determines the energy reconstruction, and any attenuation will lead to an error in energy determination and a degradation in resolution due to loss of signal-to-noise ratio. It may also lead to a reduction in efficiency, especially for short and minimum ionizing tracks. In a previous publication [20], we constructed a model for describing the dynamics of impurity concentrations in

LAr detectors and their dependence on materials of construction and operating conditions. In this paper we analyze the relation between impurity concentrations and electron drift lifetimes.

In LAr containing an impurity with an electron affinity (often loosely characterized as an electronegative impurity¹), the charge Q of the electrons in a swarm decreases exponentially with time as it drifts [22]:

$$\frac{dQ}{dt} = -k_A \cdot n \cdot Q, \quad (1.1)$$

$$Q(\tau_D) = Q(0) \cdot e^{-k_A \cdot n \cdot \tau_D}, \quad (1.2)$$

where n is the concentration of the impurity, $Q(0)$ is the initial charge of the electron swarm, $Q(\tau_D)$ is the charge after drifting for a time τ_D , and k_A is the electron attachment rate constant for the impurity in LAr. This equation is also the basis of operation for the ICARUS purity monitor [23, 24]. The mean lifetime of the charge cluster is

$$\tau_A = \frac{1}{k_A \cdot n}, \quad (1.3)$$

which is referred to as the electron lifetime. The attenuation length λ_A is defined as:

$$\lambda_A = v_D \cdot \tau_A = \frac{v_D}{k_A \cdot n}, \quad (1.4)$$

where v_D is the electron drift velocity in LAr. The drift velocity as a function of electric field used here was obtained from a global fit to the literature as described in Ref. [25].

The electron attachment rate constant is an integral over energy of the product of the drifting electron energy distribution function and the cross section for the attachment of the electron to an impurity molecule, both of which are functions of the drifting electron energy. Therefore, k_A is a function of the external electric field. For electric fields below about 100 V/cm, the electrons are in thermal equilibrium with the liquid² and in this region the electron energy distribution function (EEDF) is independent of electric field. Therefore the attachment rate is independent of the electric field at low fields. Also, in the low field limit the drift velocity is proportional to the electric field (i.e. the mobility is constant), so λ_A is simply proportional to the field.

In this paper, we summarize measured electron attachment rate constants reported in the literature for six impurities in LArTPC as a function of the external electric field. We further provide analytical functions that parameterize this data, which can be used to interpolate between measured points to compare with new measurements. Such interpolation can be particularly useful for converting lifetimes measured with a purity monitor operating at low field (in order to extend their dynamic range to longer lifetimes) to the lifetime at the operating field of the TPC.

2. Global Fit to existing Data

2.1 Data from the literature

The data sets for different impurity species are summarized in Table. 1. The data presented and discussed here were extracted from the bitmap images of the appropriate graphs in the PDF files

¹Electronegativity measures the relative attraction of a given atom for the shared electrons when forming a molecule in a chemical bond (see [21]). Therefore molecules cannot be assigned electronegativities. Electron affinity is the binding energy of the electron in a negative ion of an atom or molecule, each in its ground state.

²The electron energy is proportional to the transverse diffusion, which is constant at low electric fields. See [25].

obtained from the journal websites for each of the papers listed in Table. 1. Each bitmap image was imported into a drawing program (CorelDraw). By enlarging the image, it was straightforward to make an accurate estimate of the centroid of the pixels comprising each data point symbol. The coordinates of the vertices of the lines segments representing the data, error bars, and axes were digitized and scaled to the domain and range on the original axes as indicated in the respective publications.

The attachment rate constants k_A are given explicitly only by Bakale, *et al.* [22] and by Adams, *et al.* [26]. For the remainder of the literature the attachment rate constants are derived from the data provided. In Bettini, *et al.*[23] and Hofmann, *et al.* [27] electron lifetimes τ_A and attenuation lengths λ_A , respectively, are plotted as a function of electric field E . These can be converted to attachment rates using an inversion of Eq. 1.3. Biller *et al.*[28] gives plots of inverse attenuation lengths λ_A^{-1} as a function of added oxygen concentration. Each of these data sets was fitted with a straight line to extract the slope $d\lambda_A^{-1}/dn$, from Eq. 1.4, which gives the attachment rate constant divided by the drift velocity.

Concentrations of the impurity were determined by various methods in these measurements, as indicated in column 4 of Table 1. The designation "volumetric" means that a known volume of the impurity gas was introduced into the cryostat containing a known volume of LAr. The assumption was made that all of the impurity entered the liquid. In equilibrium, an impurity will distribute between the gas and liquid in the ratio

$$H_{xx} = \frac{n_{Gas}}{n_{Liq}}, \quad (2.1)$$

which is known as Henry's coefficient. We express all concentrations as mole fractions (moles of impurity per mole of LAr), since concentrations expressed in these units are independent of the thermodynamic state (pressure, temperature, solid, liquid, gas) of the solution. Attachment rate constants then have the units of s^{-1} and Henry's coefficient is dimensionless. For a detailed discussion on the role of Henry's coefficient in the distribution of impurities in LAr see [20].

Table 1. Data for the global fit of attachment rate

Data Set	Impurities	Data Type	n from	Ref
Biller, <i>et al.</i>	O ₂ and N ₂	λ_A^{-1} vs. n for E	volumetric	[28]
Bakale, <i>et al.</i>	O ₂ , N ₂ O, and SF ₆	k_A vs. E for n	volumetric	[22]
Bettini, <i>et al.</i>	O ₂ and CO ₂	τ_A vs. E for n	volumetric	[23]
Hofmann, <i>et al.</i>	O ₂ and N ₂	λ_A vs. E for n	gas / H_{xx}	[27]
Adams, <i>et al.</i>	O ₂	k_A vs. T for E	volumetric	[26]
Carls, <i>et al.</i>	H ₂ O	τ_A and n at E	liquid	[29]

For the four cases labeled "volumetric" in the table, the assumption that Henry's coefficient is zero leads to a very small error since the volume and density of the gas were always much smaller than those of the liquid and Henry's coefficient for all these gases is probably not much larger than 1. In the measurements of Hofmann, *et al.* the concentration in the gas is directly measured, and this value is converted to that in the liquid by dividing by Henry's coefficient for O₂, which is 0.91[20]. From the description of the procedure in the paper, it seems reasonable that the sampled gas and

the liquid are in equilibrium. In the measurement of Carls, *et al.* the concentration in the liquid was determined by converting the liquid to gas in a tube terminating in the liquid and measuring the concentration in the resulting gas.

As an example, data from Biller *et al.* [28] for O₂ can be converted to

E (kV/cm)	$k_A \pm 1\sigma (s^{-1})$
0.50	$(2.79 \pm 0.20) \times 10^{12}$
1.00	$(2.22 \pm 0.13) \times 10^{12}$
1.50	$(1.85 \pm 0.08) \times 10^{12}$
2.00	$(1.56 \pm 0.05) \times 10^{12}$
3.00	$(1.04 \pm 0.06) \times 10^{12}$

The rest of the data extracted from the literature can be found in the Appendix. All the data are shown in Fig. 1 as colored points with error bars, if available.

We found two papers that provide lifetime and concentration measurements for water in LAr. The first of these, (Andrews, *et al.* [30]), reports measured water concentration in the gas. For these measurements, the conditions of the sampled gas appear to be far from equilibrium with the liquid, and it is difficult to relate, with confidence, the measured gas concentrations to those in the liquid, so we did not use this data. However, in the second paper (Carls, *et al.* [29]), which gives water and oxygen concentration data taken after the initial filling of the MicroBooNE cryostat, the LAr is sampled with a tube dipping into the liquid. The liquid is converted to gas as it travels up the tube, and the concentration of water in this gas is measured as described in the paper. If the evaporation is done in the “sudden” (thermodynamically adiabatic³) limit, then the measured gas concentration is that of the liquid. Figure 2 in the paper displays the concentrations of oxygen and water in the LAr during a period of 18 days following the start of re-circulation of the LAr through a purifier. Figure 6 is a plot of the charge attenuation over the drift distance of an ICARUS purity monitor (20 cm). This graph also marks the charge attenuation ratios corresponding to 3 ms, 6 ms, and 9 ms. We have used these three points to establish a logarithmic scale, as required by Eq. 1.1, to convert the charge ratios to lifetimes. There are 25 points in this lifetime data set, during the interval between 13 and 18 days, in common with the concentration data set. For the time of each point in the concentration data set we have obtained the corresponding lifetime, and for each pair of values we computed the attachment rate constant, using Eq. 1.3. The mean and standard deviation of these values gives an attachment rate constant for water in LAr of $(7.80 \pm 1.5) \times 10^{10} s^{-1}$ at an electric field of 32 V/cm. This electric field is not stated in the paper; we have deduced it from the stated drift time and length using the value of the electron mobility in LAr[25].

Two processes can cause significant systematic uncertainties in the above evaluation of the attachment rate from the MicroBooNE data set [29]. The first arises from the facts that the purity monitor and the sampling point are at some distance from each other and that the water concentration is not uniformly distributed throughout the entire volume. We assign $\pm 20\%$ for this uncertainty. The second is that oxygen may contribute to the measured lifetime. The oxygen concentration measurement fell below the detection threshold of 100 ppt after 6.5 days and remains there for the remainder of the measurement. We therefore estimate a residual concentration less

³For the design of an adiabatic liquid sampling system see [31].

than 10 ppt of oxygen; removing this would systematically lower the attachment rate of water by 10%. The sum in quadrature of these two systematic uncertainties is represented in the error bar for the data point for attachment to water shown in Fig. 1.

A third systematic uncertainty arises from the possibility that the evaporation occurred under conditions at or near equilibrium between the liquid and gas (as is the case if the two fluids remain in good thermal contact and the evaporation rate per contact area is small), in which case the concentration measured in the gas will be Henry's coefficient times the concentration in the liquid, and the above attachment rate coefficient must be multiplied by this factor.

Unfortunately, the value of Henry's coefficient for H₂O in LAr has not been measured. However, an estimated value is reported by the NIST program REFPROP v10, using an EOS model fitted to a large body of data; this value is 4.1×10^{-3} at 90 K[32]. If this estimate for Henry's coefficient were correct, then we would find an attachment rate of $3.2 \times 10^8 \text{ s}^{-1}$. This should be considered as a lower limit on the true value consistent with this data, since it is likely that the sampling was in fact more nearly adiabatic than equilibrium, and the true value is probably much closer to the larger value quoted above. To represent this uncertainty, we do not include it in the stated value but indicate it in Fig.1 as an arrow pointing to the lower limit.

2.2 Fitting Functions

The attachment rate data is fit with a constrained rational polynomial:

$$k_A = 10^p \cdot \frac{\frac{a_1}{b_1} + a_1 E + a_2 E^2 + a_3 E^3 + a_4 E^4}{1 + b_1 E + b_2 E^2 + b_3 E^3 + b_4 E^4} \quad (2.2)$$

where E is the electric field in units of kV/cm and k_A is the attachment rate constant in units of s^{-1} , p is a scaling factor introduced to keep the values being fitted close to unity. The term $\frac{a_1}{b_1}$ in the numerator ensures that $\lim_{E \rightarrow 0} \frac{dk_A}{dE} = 0$. This constraint is imposed to force the fit function to be constant at low field, as attachment rate constants must be.

We have chosen to use rational polynomial functions, rather than simple polynomial functions, to fit the attachment data, motivated by the unique capabilities of Padé approximants in optimally representing mathematical functions. In general, compared to simple polynomials, rational polynomials 1) can produce a larger variety of shapes; 2) are less oscillatory, providing more credible interpolation between data points; 3) can easily be designed to conform to a priori behavior outside the domain of the data, providing more useful extrapolation; 4) can model complicated behavior with fewer terms including both the numerator and denominator, allowing more degrees of freedom for a given data set.

The potential disadvantage of using rational polynomials to fit data is that the best fit function can result in a pole (a root in the denominator) between two adjacent data points, making interpolation in the region between these two points useless. Any poles can be observed easily in a plot of the fitted function. They can then be eliminated by reducing the degree of the denominator, sometimes at the expense of increasing the chi-square value for the fit.

The coefficients of the best-fit rational polynomial obtained for each impurity are listed in Table 2. Coefficients of terms set to zero in the table indicate that including these terms either results in introducing a pole between data points, or does not reduce the value of χ^2 per degree of freedom. There is no fit for the water data, since there is only one point.

Table 2. Parameters for the best fit to data of Table 1 using Eq. 2.2

Parameters	Molecule				
	SF ₆	N ₂ O	O ₂	CO ₂	N ₂
p	16	14	11	11	10
a ₁	37.8289	0.0569772	39.4	2.20137	6.69454 × 10 ⁶
a ₂	268.031	0.781486	1.20062	12.101	-1.1286 × 10 ⁶
a ₃	45.3633	-0.0131373	0	0	0
a ₄	0	8.24298 × 10 ⁻⁵	0	0	0
b ₁	23.3285	2.89403	0.925794	1.26191	2.00731 × 10 ⁷
b ₂	355.388	0.0970965	1.63816	0	0
b ₃	160.07	0	0	0	0
b ₄	2.83519	0	0	0	0

The best fit function for each impurity is shown by the thick black solid lines in Fig.1. The uncertainty bands for the fits, at the 95% confidence level, are shown as the thin black lines.

3. Applications

It has been demonstrated by ICARUS [33], MicroBooNE [29], and ProtoDUNE [34] that a very high electron lifetimes (>15-30 ms) can be achieved. Our fits with the parameters shown in Table. 2 can be used to predict the electron lifetime as a function of electric field for different oxygen concentrations as shown in Fig. 2. It is clearly demonstrated that a sub-ppb purity level is required to achieve an electron lifetime of over 1 ms in a LArTPC. This application only considers a single impurity of O₂. In case the concentration of each individual impurity species can be determined, one can derive the corresponding attachment rate constant for that mixture. For large attenuation lengths, the charge attenuation as described in Eq. (1.1) is small. The precision of the charge attenuation determination is then limited by measurement techniques [29]. To improve the precision of charge attenuation determination, one strategy is to measure the attenuation at a lower electric field, so that the effect can be significantly increased and thus better measured. But this requires an accurate extrapolation from the low electric field setting to the nominal electric field setting. Such an extrapolation requires a knowledge of the amount of the various impurities in the LAr. The parameterizations of the attachment coefficients are particularly useful in solving the following problems.

1. If we know the the concentrations of one or more impurities, then we can use the parameterization functions to compute the partial lifetime, or attenuation length, for that set of impurities at any electric field. At low fields, where attachment rate is independent of field, the constants listed in Table. 3 can be used instead: for each impurity in column 1, the attachment rates $k_{A,0}$ is given in column 2, and the conversion factors to obtain lifetime, $\tilde{\tau}_{A,0}$, and attenuation length, $\tilde{\lambda}_{A,0}$, are given in columns 4 and 5, respectively. The ratio $k_{A,500}/k_{A,0}$ (in column 5) is the conversion factor for a purity monitor operating at voltage below the nominal 500 V/cm drift field, which will be discussed in the following paragraphs. The factor $\tilde{\tau}_{A,0}$, when divided by the impurity concentration in ppb, gives the lifetime τ in ms; the factor $\tilde{\lambda}_{A,0}$, when

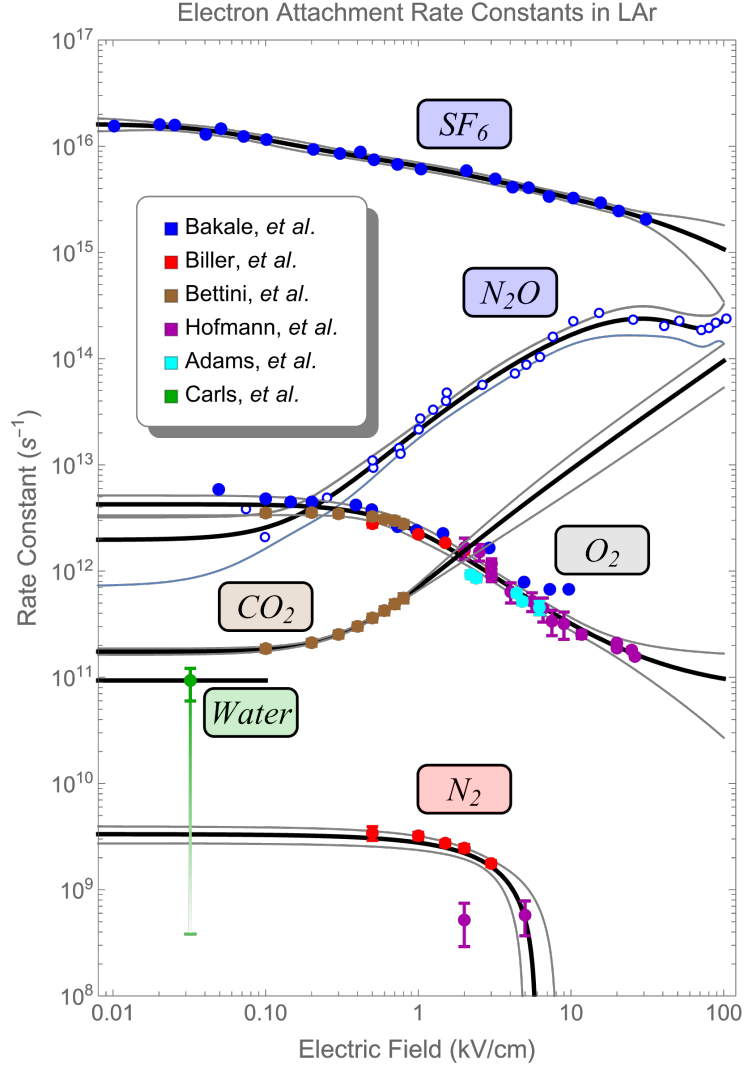


Figure 1. The electron attachment rate constant as a function of the applied electric field for six impurities in LAr at 90K. The heavy solid lines are the best-fit curves using the parameters in Table 2, and the light lines indicate the 95% confidence uncertainty bands for the fit. Open circles are used for the N_2 Bakale data to distinguish them from the nearby O_2 Bakale data. The numerical value for each data point can be found in the Appendix.

multiplied by the field in V/cm and divided by the concentration in ppb, gives the attenuation length λ in cm. The maximum field E_{\max} , in V/cm, for which these zero field constants are accurate, within the stated uncertainties, are given in column 6.

2. We can convert measured lifetimes to an "oxygen equivalent" concentration or to any other "impurity equivalent", or given a set of concentrations (as for example air) we can compute the "impurity equivalent" concentration for that mixture.
3. When the LAr becomes very pure, the purity monitor (PM) cannot accurately measure lifetimes because the attenuation length of the electron swarm becomes longer than the drift

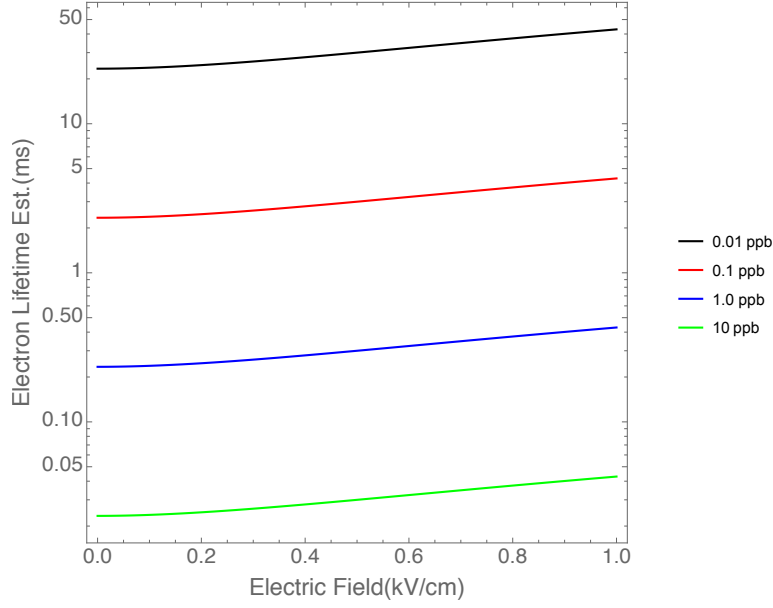


Figure 2. Electron lifetime prediction τ_A as a function of electric field for $[O_2]$ of 0.01, 0.1, 1.0, 10.0 ppb.

Table 3. Quantities characterizing attachment at zero field.

Molecule	$k_{A,0}(\text{ms ppb})^{-1}$	$\tilde{\tau}_{A,0}(\text{ms ppb})$	$\tilde{\lambda}_{A,0}(\text{cm}^2\text{V}^{-1}\text{ppb})$	$k_{A,500}/k_{A,0}$	$E_{\text{max}}(\text{V cm}^{-1})$
SF ₆	$(1.62 \pm 0.28) \times 10^4$	$(6.2 \pm 1.1) \times 10^{-5}$	$(3.3 \pm 0.7) \times 10^{-5}$	0.47 ± 0.09	26
N ₂ O	2.0 ± 0.6	0.51 ± 0.15	0.27 ± 0.09	5.0 ± 1.6	87
O ₂	4.3 ± 0.9	0.23 ± 0.05	0.126 ± 0.031	0.79 ± 0.19	332
CO ₂	0.174 ± 0.012	5.7 ± 0.4	3.1 ± 0.4	2.06 ± 0.15	93
H ₂ O	$0.093^{+0.028}_{-0.033}$	$10.7^{+3.2}_{-4.}$	$5.7^{+1.9}_{-2.2}$	$1.0^{+0.4}_{-0.5}$	n/a
N ₂	0.0033 ± 0.0006	$300. \pm 54.$	$161. \pm 36.$	0.92 ± 0.22	801

length of the PM, and then the attenuation of the charge is less than the uncertainties in the two charge measurements. We can avoid this limitation by operating the purity monitor at a lower electric field and then converting the observed low field lifetime to the lifetime at the operating field of the TPC. For the typical operating field of 500 V/cm, the conversion factors $k_{A,500}/k_{A,0}$ (given in column 5) can be used. Again, these factors are only applicable if the reduced field is lower than the maximum field E_{max} .

4. When we have observed an attenuation length that is longer than the length of the PM, then we can compute the field to use for the purity monitor to obtain the most accurate measurement on the lifetime (attenuation length). It is straightforward to show that if the PM operation is described simply by Eq. 1.1, and if the uncertainty in the value of the initial (cathode) and final (anode) charge are equal, then the minimum uncertainty in the determination of the lifetime occurs when the lifetime is slightly less than one half of the drift time. Reducing the field to achieve this condition is limited by the fact that when the field is too low the longitudinal diffusion time of the swarm will exceed the shaping time of the charge amplifier. This will

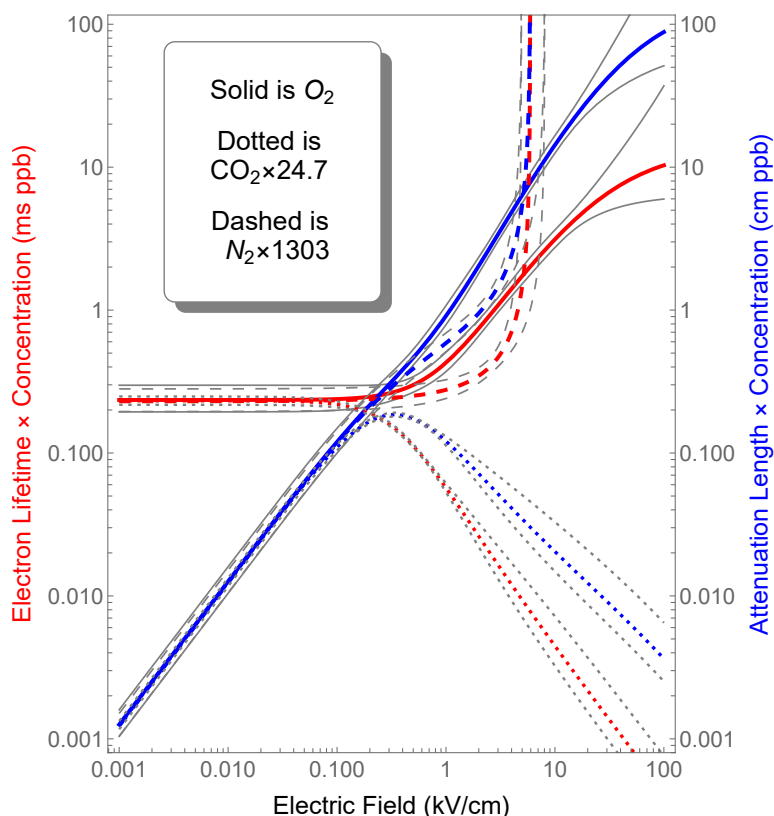


Figure 3. Electron lifetime in ms times concentration in ppb (red) and attenuation length in cm times concentration in ppb (blue) prediction as a function of electric field for $[O_2]$ (solid), CO_2 (dotted), and N_2 (dashed). Note that the curves for CO_2 and N_2 have been scaled to make allow a direct comparison of the field dependencies.

result in a systematic reduction in the measured charge at the cathode and an erroneously low value of attenuation length. In addition, at very low fields, the increase of the effect of diffusion on grid transparency will also lead to systematically low values of the attenuation length. These two systematic effects can be mitigated and corrected for by appropriate design of the instrumentation and by modeling of the effects. Finally, the reduction in cathode quantum efficiency at low fields (see Fig. 9 of [25]) will result in an increased uncertainty in charge measurement and therefore in attenuation length determination. It is beyond the scope of this paper to attempt to quantify the lowest useful field.

5. Since the various impurities have a somewhat different dependence of attachment rate constants on field, if we measure the lifetime over a range of fields, we can in principle solve the resulting set of linear equations to determine the concentrations of each of a set of impurities whose attachment rate constants are known. The field dependencies of three impurities are compared in Fig.3. Unfortunately the two most common impurities - nitrogen and oxygen - have a very similar dependence on field below about 300 V/cm. An impurity of interest, but not often reported, might be carbon dioxide, since the ICARUS group has observed [35] that

the dominant impurities in typical commercial LAr are oxygen, nitrogen, and carbon dioxide. Measurements of lifetimes at fields above 1 kV/cm should be able to distinguish these three impurities.

6. When we know the concentrations of a set of impurities, we can compute the partial lifetime due to these and compare it to the total lifetime measured by the PM to determine if there is any evidence for impurities other than those whose concentrations we have measured. The missing amount of the unknown impurity can be expressed as an oxygen-equivalent concentration, or simply as an unassigned partial lifetime.

4. Conclusions

In this paper, we summarize the electron attachment rate constants as a function of the external electric field for common impurities in an LArTPC with data obtained from the literature. We further provide analytical functions to parameterize existing data, which are useful when comparing measurements. Examples of applying these parameterizations to make extrapolations are presented.

Acknowledgments

This work is supported by Brookhaven National Laboratory and U.S. Department of Energy, Office of Science, Office of High Energy Physics under contract number DE-SC0012704.

References

- [1] H.H. Chen, P.E. Condon, B.C. Barish, and F.J. Sciulli. A Neutrino detector sensitive to rare processes. I. A Study of neutrino electron reactions. *FERMILAB-PROPOSAL-0496*, 5 1976.
- [2] C. Rubbia. The Liquid Argon Time Projection Chamber: A New Concept for Neutrino Detectors. *CERN-EP-INT-77-08*, *CERN-EP-77-08*, 5 1977.
- [3] W.J. Willis and V. Radeka. Liquid Argon Ionization Chambers as Total Absorption Detectors. *Nucl. Instrum. Meth.*, 120:221–236, 1974.
- [4] D. R. Nygren. The Time Projection Chamber: A New 4 pi Detector for Charged Particles. *eConf*, C740805:58, 1974.
- [5] S. Amerio et al. Design, construction and tests of the ICARUS T600 detector. *Nucl. Instrum. Meth. A*, 527:329–410, 2004.
- [6] C. Anderson et al. The ArgoNeuT Detector in the NuMI Low-Energy beam line at Fermilab. *JINST*, 7:P10019, 2012.
- [7] H. Berns et al. The CAPTAIN Detector and Physics Program. In *Proceedings, 2013 Community Summer Study on the Future of U.S. Particle Physics: Snowmass on the Mississippi (CSS2013): Minneapolis, MN, USA, July 29-August 6, 2013*, 2013.
- [8] I. Badhrees et al. Argontube: An R&D liquid Argon Time Projection Chamber. *JINST*, 7:C02011, 2012.
- [9] R. Acciarri et al. Design and Construction of the MicroBooNE Detector. *JINST*, 12(02):P02017, 2017.

- [10] Alan Hahn et al. The LBNE 35 Ton Prototype Cryostat. In *2014 IEEE Nuclear Science Symposium and Medical Imaging Conference and 21st Symposium on Room-Temperature Semiconductor X-ray and Gamma-ray Detectors*, page 7431158, 2016.
- [11] B. Abi et al. The Single-Phase ProtoDUNE Technical Design Report. , 6 2017, 1706.07081.
- [12] T. Alexander et al. DarkSide search for dark matter. *JINST*, 8:C11021, 2013.
- [13] A. Badertscher et al. ArDM: first results from underground commissioning. *JINST*, 8:C09005, 2013, 1309.3992.
- [14] Andrea Zani. The WArP Experiment: A Double-Phase Argon Detector for Dark Matter Searches. *Adv. High Energy Phys.*, 2014:205107, 2014.
- [15] M. Antonello et al. A Proposal for a Three Detector Short-Baseline Neutrino Oscillation Program in the Fermilab Booster Neutrino Beam. , 3 2015, 1503.01520.
- [16] R. Acciarri et al. Long-Baseline Neutrino Facility (LBNF) and Deep Underground Neutrino Experiment (DUNE). , 2016, 1601.05471.
- [17] C. E. Aalseth et al. DarkSide-20k: A 20 tonne two-phase LAr TPC for direct dark matter detection at LNGS. *Eur. Phys. J. Plus*, 133:131, 2018, 1707.08145.
- [18] Norman Gee, M. Antonio Floriano, Toshinori Wada, Sam S.-S. Huang, and Gordon R. Freeman. Ion and electron mobilities in cryogenic liquids: Argon, nitrogen, methane, and ethane. *Journal of Applied Physics*, 57(4):1097–1101, 1985, <https://doi.org/10.1063/1.334552>.
- [19] Peter Hammond. Benchmark energies of negative ion states of argon. *Journal of Physics B: Atomic, Molecular and Optical Physics*, 29(6):L231–L237, 1996.
- [20] Aiwu Zhang et al. Modeling impurity concentrations in liquid argon detectors. *Nucl. Instrum. Meth. A*, 1010:165491, 2021, 2009.10906.
- [21] A. D. McNaught and A. Wilkinson. Blackwell. Iupac. compendium of chemical terminology, 2nd ed. (the "gold book"), 2014. Accessed = 2022-03-31.
- [22] George Bakale, Ulrich Sowada, and Werner F Schmidt. Effect of an electric field on electron attachment to sulfur hexafluoride, nitrous oxide, and molecular oxygen in liquid argon and xenon. *The Journal of Physical Chemistry*, 80(23):2556–2559, 1976.
- [23] A Bettini, A Braggiotti, F Casagrande, P Casoli, P Cennini, S Centro, M Cheng, A Ciocio, S Cittolin, D Cline, et al. A study of the factors affecting the electron lifetime in ultra-pure liquid argon. *Nuclear Instruments and Methods in Physics Research Section A: Accelerators, Spectrometers, Detectors and Associated Equipment*, 305(1):177–186, 1991.
- [24] G Carugno, B Dainese, F Pietropaolo, and F Ptohos. Electron lifetime detector for liquid argon. *Nuclear Instruments and Methods in Physics Research Section A: Accelerators, Spectrometers, Detectors and Associated Equipment*, 292:580–584, 1990.
- [25] Yichen Li et al. Measurement of Longitudinal Electron Diffusion in Liquid Argon. *Nucl. Instrum. Meth. A*, 816:160–170, 2016, 1508.07059.
- [26] M Adams, P Buchholz, A Dahlhoff, D Feiden, V Gärtner, M Grams, M Haarmann, A Hergesell, F Hölldorfer, G Ielapi, et al. A purity monitoring system for liquid argon calorimeters. *Nuclear Instruments and Methods in Physics Research Section A: Accelerators, Spectrometers, Detectors and Associated Equipment*, 545(3):613–623, 2005.

- [27] W Hofmann, U Klein, M Schulz, J Spengler, and D Wegener. Production and transport of conduction electrons in a liquid argon ionization chamber. *Nuclear Instruments and Methods*, 135(1):151–156, 1976.
- [28] S. D. Biller, Daniel N. Kabat, R. C. Allen, G. Buehler, and P. J. Doe. Effects of oxygen and nitrogen on drifting electrons in a liquid argon TPC. *Nucl. Instrum. Meth. A*, 276:144–150, 1989.
- [29] MicroBooNE Collaboration. Measurement of the electronegative contaminants and drift electron lifetime in the microboone experiment. Technical report, MICROBOONE-NOTE-1003-PUB, May 19th, 2016. <https://www-microboone.fnal.gov> . . . , 2016.
- [30] R Andrews, W Jaskierny, H Jöstlein, C Kendziora, S Pordes, and T Tope. A system to test the effect of materials on electron drift lifetime in liquid argon and the effect of water. *Nuclear Instruments and Methods in Physics Research Section A: Accelerators, Spectrometers, Detectors and Associated Equipment*, 608(2):251–258, 2009.
- [31] GT Preston, EW Funk, and J Mi Prausnitz. Solubilities of hydrocarbons and carbon dioxide in liquid methane and in liquid argon. *The Journal of Physical Chemistry*, 75(15):2345–2352, 1971.
- [32] Nist program refprop v10,. <https://www.nist.gov/srd/refprop>. Accessed: 03/31/2022.
- [33] M. Antonello et al. Experimental observation of an extremely high electron lifetime with the ICARUS-T600 LAr-TPC. *JINST*, 9(12):P12006, 2014, 1409.5592.
- [34] B. Abi et al. First results on ProtoDUNE-SP liquid argon time projection chamber performance from a beam test at the CERN Neutrino Platform. *JINST*, 15(12):P12004, 2020, 2007.06722.
- [35] LNGS/AQ Group. Preliminary results on argon residual contaminations inside the icarus t600 cryostats. Technical report, ICARUS-TM/11-01, INFN Lab. Naz. del Gran Sasso, Assergi (Italy), 2011.

Appendix: Extracted data from the literature

Adams *et al.* data [26] for O_2 :

E (kV/cm)	$k_A \pm 1\sigma (s^{-1})$
2.20	$(9.3 \pm 0.7) \times 10^{11}$
2.40	$(8.6 \pm 0.6) \times 10^{11}$
4.40	$(6.2 \pm 0.4) \times 10^{11}$
4.80	$(5.2 \pm 0.4) \times 10^{11}$
6.20	$(4.5 \pm 0.6) \times 10^{11}$

Biller *et al.* data [28] for N_2 :

E (kV/cm)	$k_A \pm 1\sigma (s^{-1})$
0.50	$(3.4 \pm 0.5) \times 10^9$
1.00	$(3.22 \pm 0.25) \times 10^9$
1.50	$(2.74 \pm 0.18) \times 10^9$
2.00	$(2.47 \pm 0.20) \times 10^9$
3.00	$(1.77 \pm 0.11) \times 10^9$

Bakale *et al.* data[22] for N_2O (no error provided in the original figure):

E (kV/cm)	$k_A (s^{-1})$
0.07	3.83×10^{12}
0.10	2.09×10^{12}
0.25	4.91×10^{12}
0.51	9.41×10^{12}
0.50	1.10×10^{13}
0.75	1.44×10^{13}
0.76	1.27×10^{13}
1.01	2.16×10^{13}
1.03	2.73×10^{13}
1.25	3.31×10^{13}
1.52	4.00×10^{13}
1.53	4.79×10^{13}
2.63	5.67×10^{13}
4.29	7.25×10^{13}
5.10	8.78×10^{13}
6.26	1.04×10^{14}
7.60	1.61×10^{14}
10.35	2.25×10^{14}
15.26	2.70×10^{14}
25.52	2.33×10^{14}
40.78	2.04×10^{14}
51.25	2.28×10^{14}
71.38	1.86×10^{14}
80.03	1.95×10^{14}
88.69	2.18×10^{14}
104.10	2.38×10^{14}

Bakale *et al.* data[22] for O_2 (no error provided in the original figure):

E (kV/cm)	$k_A (s^{-1})$
0.05	5.87×10^{12}
0.10	4.80×10^{12}
0.15	4.49×10^{12}
0.20	4.49×10^{12}
0.39	4.19×10^{12}
0.50	3.79×10^{12}
0.73	2.62×10^{12}
0.97	2.42×10^{12}
1.45	2.26×10^{12}
2.91	1.65×10^{12}
4.92	7.88×10^{11}
7.26	6.73×10^{11}
9.66	6.73×10^{11}

Bakale data [22] for SF_6 (no error provided in the original figure):

E (kV/cm)	$k_A (s^{-1})$
0.01	1.55×10^{16}
0.02	1.60×10^{16}
0.03	1.58×10^{16}
0.04	1.29×10^{16}
0.05	1.46×10^{16}
0.07	1.24×10^{16}
0.10	1.16×10^{16}
0.21	9.35×10^{15}
0.31	8.54×10^{15}
0.42	8.84×10^{15}
0.51	7.47×10^{15}
0.73	6.75×10^{15}
1.04	6.10×10^{15}
2.07	5.90×10^{15}
3.19	4.93×10^{15}
4.15	4.12×10^{15}
5.27	4.07×10^{15}
7.18	3.37×10^{15}
10.35	3.25×10^{15}
15.62	2.94×10^{15}
20.54	2.46×10^{15}
31.00	2.05×10^{15}

Bettini *et al.* data [23] for O_2 :

E (kV/cm)	$k_A \pm 1\sigma (s^{-1})$
0.10	$(3.52 \pm 0.25) \times 10^{12}$
0.20	$(3.56 \pm 0.26) \times 10^{12}$
0.30	$(3.47 \pm 0.25) \times 10^{12}$
0.50	$(3.26 \pm 0.24) \times 10^{12}$
0.60	$(3.09 \pm 0.23) \times 10^{12}$
0.70	$(2.99 \pm 0.24) \times 10^{12}$
0.80	$(2.78 \pm 0.21) \times 10^{12}$

Hofmann *et al.* data [27] for N_2 :

E (kV/cm)	$k_A \pm 1\sigma (s^{-1})$
2.0	$(5.2 \pm 2.3) \times 10^8$
5.0	$(5.8 \pm 2.1) \times 10^8$

Bettini *et al.* data [23] for CO_2 :

E (kV/cm)	$k_A \pm 1\sigma (s^{-1})$
0.10	$(1.86 \pm 0.14) \times 10^{11}$
0.20	$(2.12 \pm 0.16) \times 10^{11}$
0.30	$(2.53 \pm 0.19) \times 10^{11}$
0.40	$(3.02 \pm 0.25) \times 10^{11}$
0.50	$(3.62 \pm 0.30) \times 10^{11}$
0.60	$(4.2 \pm 0.4) \times 10^{11}$
0.70	$(4.9 \pm 0.5) \times 10^{11}$
0.80	$(5.6 \pm 0.5) \times 10^{11}$

Carls, *et al.* data[29] for H_2O

E (kV/cm)	$k_A \pm 1\sigma (s^{-1})$
0.03	$9.3^{+2.8}_{-3.3} \times 10^{10}$

Hofmann *et al.* data [27] for O_2 :

E (kV/cm)	$k_A \pm 1\sigma (s^{-1})$
2.01	$(1.7 \pm 0.4) \times 10^{12}$
2.51	$(1.51 \pm 0.27) \times 10^{12}$
3.01	$(1.18 \pm 0.13) \times 10^{12}$
3.01	$(8.9 \pm 1.0) \times 10^{11}$
4.03	$(6.4 \pm 1.4) \times 10^{11}$
5.55	$(5.2 \pm 1.0) \times 10^{11}$
6.56	$(4.4 \pm 1.1) \times 10^{11}$
7.49	$(3.4 \pm 0.9) \times 10^{11}$
8.98	$(3.2 \pm 0.9) \times 10^{11}$
11.72	$(2.53 \pm 0.21) \times 10^{11}$
19.95	$(2.11 \pm 0.06) \times 10^{11}$
19.98	$(1.88 \pm 0.09) \times 10^{11}$
24.94	$(1.81 \pm 0.09) \times 10^{11}$
26.20	$(1.57 \pm 0.07) \times 10^{11}$